

Exclusive production of T_{cc}^- in hadron-hadron ultraperipheral collisions

Xiao-Peng Wang,^{1,2,3} Ya-Ping Xie,^{1,3} Yin Huang,^{4,*} and Xu-Rong Chen^{1,3,†}

¹*Institute of Modern Physics, Chinese Academy of Sciences, Lanzhou 730000, China*

²*School of Nuclear Science and Technology, Lanzhou University, Lanzhou 730000, China*

³*School of Nuclear Science and Technology, University of Chinese Academy of Sciences, Beijing 100049, China*

⁴*School of Physical Science and Technology, Southwest Jiaotong University, Chengdu 610031, China*

(Dated: October 10, 2023)

Understanding the production mechanisms and utilizing them as probes to investigate the structure of exotic states represent some of the most actively studied research areas in particle physics. In this study, we present a theoretical analysis of the charmed meson T_{cc}^- in the $\gamma p \rightarrow D^+ T_{cc}^- \Lambda_c^+$ and $\gamma\gamma \rightarrow D^+ T_{cc}^- D^{*0}$ reactions, considering T_{cc}^+ as a DD^* molecule. The differential cross-section and total cross-section for the photoproduction of T_{cc}^- in the $\gamma p \rightarrow D^+ T_{cc}^- \Lambda_c^+$ and $\gamma\gamma \rightarrow D^+ T_{cc}^- D^{*0}$ reactions are presented for nucleus-nucleus (nucleon-nucleon) ultraperipheral collisions at HL-LHC and RHIC, respectively. Taking into account the integrated luminosity per typical run and the luminosity of photons from the nucleus (nucleon), we observe a significant event count for T_{cc}^- production in p-p ultraperipheral collisions at HL-LHC.

I. INTRODUCTION

The quark model offers a convenient framework for classifying hadrons, effectively encompassing the majority of hadronic states. Nonetheless, significant experimental advancements have been made in recent years, leading to the observation of numerous exotic hadrons [1, 2]. These exotic mesons exhibit an internal structure more complex than the simple $q\bar{q}$ configuration for mesons or qqq configuration for baryons in the traditional constituent quark models.

The study of exotic hadrons has a long and storied history. However, it entered a new and exciting era in 2003 when the Belle collaboration made a groundbreaking discovery of the $X(3872)$ in the $\pi^+\pi^-J/\psi$ mass spectra [3]. The $X(3872)$, based on its observed decay mode, is known to consist of at least four distinct valence quarks, making it a candidate for an exotic hadron. Another well-known exotic hadron candidate is the charged-particle $Z_c^+(3900)$, which was initially observed by the BESIII collaboration in the $\pi^\pm J/\psi$ mass spectrum [4]. This observation was later confirmed by the Belle collaboration in the process $e^+e^- \rightarrow \pi^+\pi^-J/\psi$ [5]. Moreover, the LHCb Collaboration has made significant strides in the field by reporting several hidden-charm pentaquark states [6, 7].

These discoveries have garnered significant attention towards exotic hadron states, particularly those containing charm quarks. Notably, it brings to mind the double-charm meson T_{cc}^+ , which was observed by the LHCb Collaboration in the $D^0 D^0 \pi^+$ invariant mass spectrum [8]. The T_{cc}^+ meson's mass, width, and quantum numbers

were precisely measured as follows:

$$\begin{aligned} M &= 3875.09 \text{ MeV} + \delta m, \\ \Gamma &= 48 \pm 2_{-14}^{+0} \text{ KeV}, \quad I(J^P) = 0(1^+). \end{aligned} \quad (1)$$

Since the mass of T_{cc}^+ lies just below the nominal $D^{*+}D^0$ threshold, it can be interpreted as a hadronic molecule [9–16]. It was worth noting that the compact multi-quark structure for T_{cc}^+ are also proposed in Refs. [17, 18].

Theoretical investigations on production mechanisms and further experimental information on production cross section will be helpful to distinguish which inner structure of the T_{cc}^+ state is possible. This dependence arises primarily from the fact that the different yields are strongly influenced by the internal structure of the hadrons. Presently, the photoproduction of T_{cc}^- , which serves as the antiparticle to T_{cc}^+ , has undergone investigation as documented in Ref. [19]. The process $\gamma p \rightarrow D^+ T_{cc}^- \Lambda_c^+$ involves the utilization of the central diffractive mechanism. In their consideration, the reaction channel involves the exchange of $D^{(*)}$ mesons in the t -channel, while the s - and u -channels are significantly suppressed due to the involvement of two additional $c\bar{c}$ pair creation. Their findings reveal that the total cross-section for $\gamma p \rightarrow D^+ T_{cc}^- \Lambda_c^+$ is approximately 1 Pb.

When compared to the lower production cross-section of the $\gamma p \rightarrow D^+ T_{cc}^- \Lambda_c^+$ reaction shown in Ref. [19], ultraperipheral collisions (UPCs) can significantly increase the probability of T_{cc}^- production [20–24]. In UPCs, electromagnetic interactions dominate, occurring when the impact parameter of two ions exceeds the sum of their radii. By employing the Weizsäcker – Williams method [21, 24, 25], the electromagnetic field originating from highly-charged nuclei can be treated as an equivalent flux of photons. As the photon flux is directly proportional to the charge number of ions, highly-charged ions offer a substantial photon number density. This suggests that if the $\gamma p \rightarrow D^+ T_{cc}^- \Lambda_c^+$ reaction occurs in ultraperipheral collisions, there will be a significant increase in the probability of T_{cc}^- production. Moreover, we also proposed to

* huangy2019@swjtu.edu.cn (Corresponding author)

† xchen@impcas.ac.cn (Corresponding author)

observe two-photon scattering [24] ($\gamma\gamma \rightarrow D^+T_{cc}^-D^*$) as another part of the search for the T_{cc}^- in UPCs due to the fact that $Z(3930)$, $X(3915)$, and $X(4350)$ were observed in this process by Belle collaboration [26–28]. As a result, UPCs serve as a crucial platform for investigating the photoproduction of the T_{cc}^- [29, 30].

This paper is organized as follows. Theoretical frameworks for the production of T_{cc}^- in $\gamma p \rightarrow D^+T_{cc}^-\Lambda_c^+$ and $\gamma\gamma \rightarrow D^+T_{cc}^-D^*$ in UPCs are presented in Section II, respectively. The numerical calculations are given in Section III. Finally, a conclusion is given in section IV.

II. THEORETICAL FRAMEWORK

In this work, we investigate the production of T_{cc}^- through one-photon and two-photon processes of ultra-peripheral collisions (UPCs). The corresponding Feynman diagrams are depicted in Figs. 1 and 2. We can find that the high-luminosity photon flux is first emitted from the nucleus or nucleon, resulting in the creation of a pair of high-energy \bar{D}^*D mesons. Due to the attractive interaction between \bar{D}^* and D , a T_{cc}^- molecule is formed in the final state. Next, we will discuss in detail the production mechanisms of T_{cc}^- , corresponding to Figs. 1 and 2, respectively.

A. The production of T_{cc}^- in one-photon process

Within the framework of UPCs, the production cross-section of $A(p)p \rightarrow D^+T_{cc}^-\Lambda_c^+A(p)$ reaction was given [31, 32],

$$\sigma(Ap \rightarrow AD^+T_{cc}^-\Lambda_c^+) = \int dk \frac{dN_\gamma(k)}{dk} \sigma_{\gamma p \rightarrow D^+T_{cc}^-\Lambda_c^+}(W), \quad (2)$$

where $\frac{dN_\gamma(k)}{dk}$ is photon flux, with the k representing the energy of the photon emitted from the nucleus (nucleon). W is the center of mass energy of the photon and proton system. Note that $W = \sqrt{2k\sqrt{s}}$ can be determined based on k and the total energy s of the system. Simplifying, we obtain the W -dependent differential cross-section

$$\frac{d\sigma}{dW} = \left(\frac{dN_\gamma(k)}{dk} \frac{W}{\sqrt{s}} \right) \sigma_{\gamma p \rightarrow D^+T_{cc}^-\Lambda_c^+}(W). \quad (3)$$

In order to make a reliable prediction for the cross-section of the $A(p)p \rightarrow D^+T_{cc}^-\Lambda_c^+A(p)$ reaction, we need to address the follow two key issues: the value of the photon flux and the $\sigma_{\gamma p \rightarrow D^+T_{cc}^-\Lambda_c^+}(W)$. The photon flux from the nucleus is described by the equation [33]

$$\frac{dN_\gamma(k)}{dk} = \frac{2Z^2\alpha_{em}}{\pi k} \left(\xi K_0(\xi) K_1(\xi) - \frac{\xi^2}{2} [K_1^2(\xi) - K_0^2(\xi)] \right), \quad (4)$$

where K_0 and K_1 are modified Bessel functions, Z is the ion charge, $\alpha_{em} = 1/137$, $\xi = b_{\min}k/\gamma_L$ with $\gamma_L = \sqrt{s}/(2m_p)$ represents the Lorentz boost factor. The value

of $b_{\min} = R_A + R_p$ is the sum of the nucleus and proton charge radius, where R_A is often defined as [34]

$$R_A = (1.12A^{1/3} - 0.86A^{-1/3}) \text{ (fm)}. \quad (5)$$

It is important to note that the photon flux emitted from the proton differs from the photon flux from the nucleus, and it can be expressed using the dipole form factor [21, 35]

$$\frac{dn}{dk}(k) = \frac{\alpha_{em}}{2\pi k} \left[1 + \left(1 - \frac{2k}{\sqrt{s}} \right)^2 \right] \times \left(\ln \Omega - \frac{11}{6} + \frac{3}{\Omega} - \frac{3}{2\Omega^2} + \frac{1}{3\Omega^3} \right), \quad (6)$$

where $\Omega = 1 + 0.71, \text{ GeV}^2/Q_{\min}^2$, and $Q_{\min}^2 = k^2/\gamma_L^2$ represents the minimum momentum transfer possible in the reaction.

The differential cross section in the c.m. frame for the $\gamma p \rightarrow D^+T_{cc}^-\Lambda_c^+$ reaction reads

$$\begin{aligned} d\sigma(\gamma p \rightarrow D^+T_{cc}^-\Lambda_c^+) &= \frac{1}{(2\pi)^5} \frac{1}{4(k_1 \cdot k_2)} \sum_{s_i, s_f} | -i\mathcal{M}(\gamma p \rightarrow D^+T_{cc}^-\Lambda_c^+) |^2 \\ &\times \frac{d^3\vec{p}_1}{2E_1} \frac{d^3\vec{p}_2}{2E_2} \frac{d^3\vec{p}_3}{2E_3} \delta^4(k_1 + k_2 - p_1 - p_2 - p_3), \end{aligned} \quad (7)$$

where E_1, E_2, E_3 and p_1, p_2, p_3 stand for the energies and four momentum of D^+, T_{cc}^- , and Λ_c^+ , respectively. k_1 and k_2 are the four momentum of the initial photon and proton, respectively, and m_p and $m_{\Lambda_c^+}$ are the masses of the proton and Λ_c^+ , respectively. The $\mathcal{M}(\gamma p \rightarrow D^+T_{cc}^-\Lambda_c^+)$ represents the total scattering amplitude for the $\gamma p \rightarrow D^+T_{cc}^-\Lambda_c^+$ reaction, which has been computed in Ref. [19]

$$\begin{aligned} -i\mathcal{M} &= \bar{u}(p_3, \lambda_{\Lambda_c^+}) \sum_{j=a,b,c} \mathcal{W}_j^{\mu\nu} u(k_2, \lambda_p) \\ &\times \epsilon_\nu(k_1, \lambda_\gamma) \epsilon_\mu^*(p_2, \lambda_{T_{cc}^-}), \end{aligned} \quad (8)$$

with

$$\begin{aligned} \mathcal{W}_a^{\mu\nu} &= -g_{D^*D} g_{D N \Lambda_c} g_{T_{cc}} \gamma_5 \epsilon_{\alpha\nu\beta\rho} k_1^\alpha q_1^\beta \\ &\times \frac{-g^{\mu\rho} + q_1^\mu q_1^\rho / m_{D^*}^2}{q_1^2 - m_{D^*}^2} \frac{\mathcal{F}_{D^*0} \mathcal{F}_{D^*-}}{q_2^2 - m_{D^*}^2}, \end{aligned} \quad (9)$$

$$\begin{aligned} \mathcal{W}_b^{\mu\nu} &= -ie g_{D^*N\Lambda_c} g_{T_{cc}} \gamma_\rho (q_1^\nu - p_1^\nu) \\ &\times \frac{-g^{\mu\rho} + q_2^\mu q_2^\rho / m_{D^*0}^2}{q_2^2 - m_{D^*0}^2} \frac{\mathcal{F}_{D^*0} \mathcal{F}_{D^-}}{q_1^2 - m_{D^-}^2}, \end{aligned} \quad (10)$$

$$\begin{aligned} \mathcal{W}_c^{\mu\nu} &= -i2e g_{D^*N\Lambda_c} g_{T_{cc}} (-\gamma_\mu + \frac{m_p - m_{\Lambda_c^+}}{m_{D^*0}^2} q_{2\mu}) \\ &\times \frac{k_1^\nu - p_1^\nu}{q_2^2 - m_{D^*0}^2} \frac{\mathcal{F}_{D^*0} \mathcal{F}_{D^-}}{q_1^2 - m_{D^-}^2}, \end{aligned} \quad (11)$$

where correspond to the Feynman diagrams as well as the contact terms discussed in Ref. [19], respectively. In the

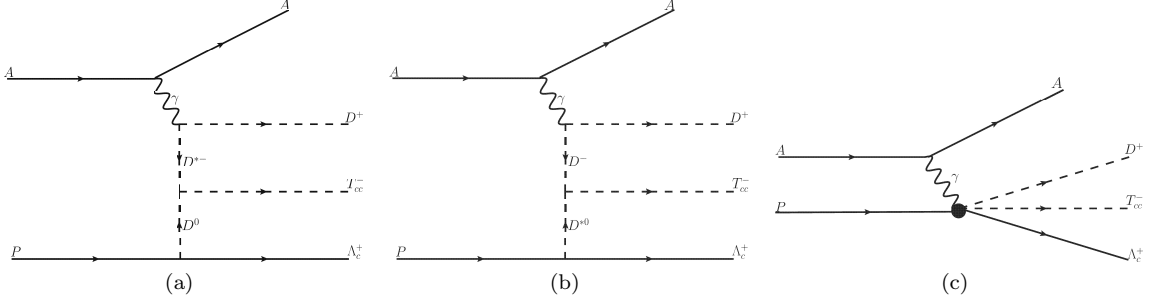


FIG. 1. Production of $p + A \rightarrow A + D^+ + T_{cc}^- + \Lambda_c^+$ and $p + p \rightarrow p + D^+ + T_{cc}^- + \Lambda_c^+$ in pA or pp UPCs.

above equation, u and ϵ are the Dirac spinor and polarization vector, respectively, and λ is the helicities. Coupling constants $g_{DN\Lambda_c} = -13.98$ and $g_{D^*N\Lambda_c} = -5.20$ are computed from the SU(4) invariant Lagrangians in terms of $g_{\pi NN} = 13.45$ and $g_{\rho NN} = 6$ [36–38]. $g_{D^*D\gamma} = 0.173 - 0.228 \text{ GeV}^{-1}$ is determined by the radiative decay widths of D^* [39]. The coupling constants $g_{T_{cc}D^*D} = 3.67 \text{ GeV}$ and $g_{T_{cc}D^0D^+} = -3.92 \text{ GeV}$ are derived from chiral unitary theory, where T_{cc} is identified as an S -wave D^*D molecule [40]. $e = \sqrt{4\pi\alpha}$ with α being the fine-structure constant, and $\epsilon^{\mu\nu\alpha\beta}$ is the Levi-Civita tensor.

Considering the internal structure of the exchange mesons, the form factor must be taken into account. In this work, the monopole form factors $\mathcal{F}_{\bar{D}^{(*)0}}$ and $\mathcal{F}_{D^{(*)-}}$ that can be found in Eqs. (9-11) are utilized, as shown in [19]

$$\mathcal{F}_i = \frac{\Lambda_i^2 - m_i^2}{\Lambda_i^2 - t_i}, \quad i = \bar{D}^0, D^{*-}, \quad (12)$$

where m_i and t_i represent the mass and the four-momentum square of exchange mesons \bar{D}^0 or D^{*-} . The cutoff $\Lambda_i = m_i + \alpha\Lambda_{\text{QCD}}$, where α is a parameter related to the nonperturbative property of QCD at the low-energy scale. In Ref. [19], $\Lambda_{\text{QCD}} = 0.22 \text{ GeV}$ is adopted, and $\alpha = 1.5$ or 1.7 is computed by fitting the experimental data [41–43].

B. The production of T_{cc}^- in two-photon process

The Feynman diagram for the production of T_{cc}^- in two-photon process of UPCs is plotted in Fig. 2. The relevant differential cross-section is expressed as

$$\frac{d\sigma_{AB}}{dW_{\gamma\gamma}} = \frac{d\mathcal{L}_{\gamma\gamma}^{AB}}{dW_{\gamma\gamma}} \sigma_{\gamma\gamma \rightarrow D^+ T_{cc}^- D^*} (W_{\gamma\gamma}), \quad (13)$$

where A and B represent the nucleus or proton. $\sigma_{\gamma\gamma \rightarrow D^+ T_{cc}^- D^*}$ denotes the total cross-section of the two-photon T_{cc}^- production process, and $W_{\gamma\gamma}$ stands for the center-of-mass energy of the two-photon system. The effective two-photon luminosity, denoted as $\frac{d\mathcal{L}_{\gamma\gamma}^{AB}}{dW_{\gamma\gamma}}$, can be

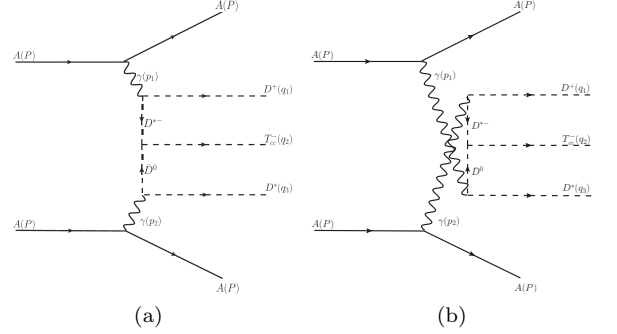


FIG. 2. Two-photon production process for T_{cc}^- in AA, pA or pp UPCs.

obtained from the gamma-UPC package [44]. However, the two-photon T_{cc}^- production cross-section is unknown and will be discussed later.

To compute the two-photon T_{cc}^- production cross-section $\sigma_{\gamma\gamma \rightarrow D^+ T_{cc}^- D^*}$, the effective Lagrangians with the smallest number of derivatives are given as follows [19, 45–48]

$$\begin{aligned} \mathcal{L}_{T_{cc}D^*D} &= g_{T_{cc}D^*D} T_{cc}^{\mu\dagger} D_\mu^* D, \\ \mathcal{L}_{\gamma DD^*} &= g_{\gamma DD^*} \epsilon_{\mu\nu\alpha\beta} (\partial^\mu \mathcal{A}^\nu) (\partial^\alpha D^{*\beta}) D + \text{H.c.}, \end{aligned} \quad (14)$$

where T_{cc}^μ , D_μ^* , D and \mathcal{A}^μ represent T_{cc}^- meson, D^* meson, D meson, and the photon, respectively.

Then, as shown in Fig. 2(a) and 2(b) for the two-photon T_{cc}^- production, the invariant amplitude of $\gamma\gamma \rightarrow D^+ T_{cc}^- D^*$ is written as

$$-i\mathcal{M} = \epsilon_\theta^*(q_3) \epsilon_\mu^*(q_2) (\mathcal{W}_{(a)}^{\theta\mu\nu\alpha} + \mathcal{W}_{(b)}^{\theta\mu\nu\alpha}) \epsilon_\nu(p_1) \epsilon_\alpha(p_2). \quad (15)$$

In the amplitude, $\mathcal{W}_{(a)}^{\theta\mu\nu\alpha}$ and $\mathcal{W}_{(b)}^{\theta\mu\nu\alpha}$ are similar. They are constructed as

$$\begin{aligned} \mathcal{W}_{(a)}^{\theta\mu\nu\alpha} &= g_a F_a \epsilon_{\beta\nu\eta\rho} p_1^\beta k_1^\eta \frac{-g^{\mu\rho} + k_1^\mu k_1^\rho / m_{D^*}^2}{k_1^2 - m_{D^*}^2} \times \\ &\quad \frac{1}{k_2^2 - m_{D^0}^2} \epsilon_{\epsilon\alpha f\theta} p_2^\epsilon q_3^f, \end{aligned} \quad (16)$$

$$\mathcal{W}_{(b)}^{\theta\mu\nu\alpha} = g_a F'_a \epsilon_{\beta\nu\eta\rho} p_2^\beta k_1^\eta \frac{-g^{\mu\rho} + k_1^\mu k_1^\rho / m_{D^*}^2}{k_1'^2 - m_{D^*}^2} \times \frac{1}{k_2'^2 - m_{\bar{D}^0}^2} \epsilon_{\epsilon\alpha f\theta} p_1^\epsilon q_3^f, \quad (17)$$

where $g_a = g_{T_{cc}D^*-\bar{D}^0} g_{\gamma D^*+D^*} - g_{\gamma\bar{D}^0 D^*}$ and $\mathcal{F}_a = \mathcal{F}_{D^*} - \mathcal{F}_{\bar{D}^0}$.

The differential cross-section for two-photon T_{cc}^- production can be described as follows

$$d\sigma_{\gamma\gamma} = \frac{1}{(2\pi)^5} \frac{1}{4\sqrt{(p_1 \cdot p_2)^2}} |\overline{\mathcal{M}}|^2 \times \delta^4(p_1 + p_2 - q_1 - q_2 - q_3) \frac{d^3\vec{q}_1}{2q_1^0} \frac{d^3\vec{q}_2}{2q_2^0} \frac{d^3\vec{q}_3}{2q_3^0}. \quad (18)$$

where $|\overline{\mathcal{M}}|$ represents the final-state spin summation and the initial-state spin averaging of the scattering amplitude. Finally, the total cross section, obtained by integrating the differential cross-section with the 3BodyXSections package [49], will be presented as a function of the center-of-mass energy W .

III. NUMERICAL RESULTS

In this study, we estimate the production cross-section of T_{cc}^- through one-photon and two-photon processes in ultra-peripheral collisions (UPCs). To achieve these results, we need to initially evaluate the cross-sections for the $\gamma\gamma \rightarrow D^+T_{cc}^-D^*$ and $\gamma p \rightarrow D^+T_{cc}^-\Lambda_c^+$ reactions, as indicated in Eqs. (3) and (13). These cross-sections can be computed by integrating the differential cross-section based on the 3BodyXSections package [49]. The equations expressing the differential cross-section for these two reactions can be found in Eqs. (7) and (18).

The cross-sections of the $\gamma p \rightarrow D^+T_{cc}^-\Lambda_c^+$ and the $\gamma\gamma \rightarrow D^+T_{cc}^-D^*$ reactions are depicted against W for $\alpha = 1.5$ and $\alpha = 1.7$ in Fig. 3 respectively. We can find that when the energy approaches the $D^+T_{cc}^-D^*$ threshold, the total cross-section increases sharply. At higher energies, the cross section increases continuously but relatively slowly compared with that near threshold. Our numerical results also show that the total cross section for $\alpha = 1.7$ is larger than that of the $\alpha = 1.5$, but the disparity is not significant. To provide an example, let's examine the cross-section at an energy of around $W = 40$ GeV. In this instance, the obtained cross-section ranges from 1.0 Pb to 1.62 Pb for $\gamma p \rightarrow D^+T_{cc}^-\Lambda_c^+$ and from 0.405 pb to 0.655 pb for $\gamma\gamma \rightarrow D^+T_{cc}^-D^*$, respectively, when altering the value of α from 1.5 to 1.7. Therefore, in the following calculations, we only provide the results with $\alpha = 1.5$. By comparing the cross-sections depicted in Fig. 3, we find that the total cross-section for T_{cc}^- production in the $\gamma p \rightarrow D^+T_{cc}^-\Lambda_c^+$ reaction is bigger than that of the T_{cc}^- production in the $\gamma\gamma \rightarrow D^+T_{cc}^-D^*$ reaction.

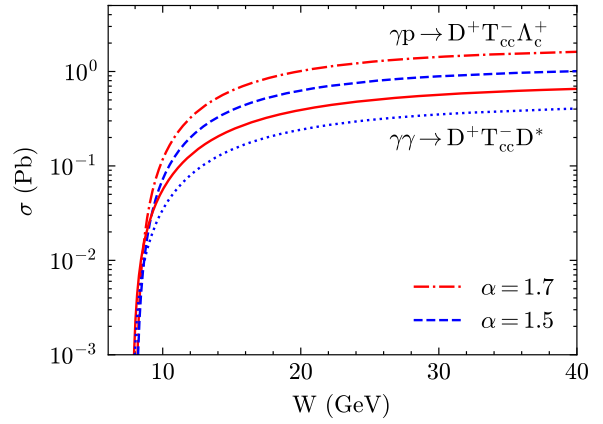


FIG. 3. Total cross sections for the $\gamma p \rightarrow D^+T_{cc}^-\Lambda_c^+$ (Dotted line and Dashed line) and for the $\gamma\gamma \rightarrow D^+T_{cc}^-D^*$ (Solid line and Dot line) as a function of W while $\alpha = 1.7$ (red line) or $\alpha = 1.5$ (blue line).

With above obtained cross-section, we present the differential cross-sections for one-photon T_{cc}^- production in ultra-peripheral collisions (UPCs) as a function of the W of the photon-nucleus system at $\sqrt{s} = 8.8$ TeV for the p – Pb system and $\sqrt{s} = 200$ GeV for the p – Au system, as illustrated in Fig. 4. We can find that the differential cross-sections for the p – Pb system are greater than those of the p – Au system. One possible explain for this is that the photon flux is directly proportional to the charge number of the nucleus. Moreover, our results suggest that the differential cross-sections are notably significant in the low-energy range. As the energy increases, the differential cross-sections decrease rapidly.

Next, we calculate the differential cross-sections through two-photon T_{cc}^- production in nucleus-nucleus and proton-proton ultra-peripheral collisions (UPCs), as illustrated in Fig. 5. These calculations are performed for collision energies of $\sqrt{s} = 5.5$ TeV for the Pb – Pb system, $\sqrt{s} = 7$ TeV for the oxygen-oxygen (O – O) system, and $\sqrt{s} = 14$ TeV for the p – p system, respectively. Moreover, for the p – Pb system and p – Au system, we present the differential cross-sections against the center-of-mass energy W , depicted in Fig. 5, for collision energies of $\sqrt{s} = 8.8$ TeV and $\sqrt{s} = 200$ GeV, respectively. It can be observed that the primary contribution of the two-photon process takes place within a distinct low center-of-mass energy range, similar to that of one-photon T_{cc}^- production. Notably, T_{cc}^- production in Pb – Pb UPCs is the largest due to the higher luminosity of the photon flux originating from Pb.

Finally, we list the predicted event numbers for one-photon and two-photon T_{cc}^- production in the Pb – Pb system, O – O system, Pb – p system, Au – p system, and p – p system, respectively, in Table. I. We can find that the total cross-section σ_{tot} for the one-photon $\gamma p \rightarrow D^+T_{cc}^-\Lambda_c^+$ process is smaller in the p – p system compared to the Pb – p and Au – p systems. However, due to

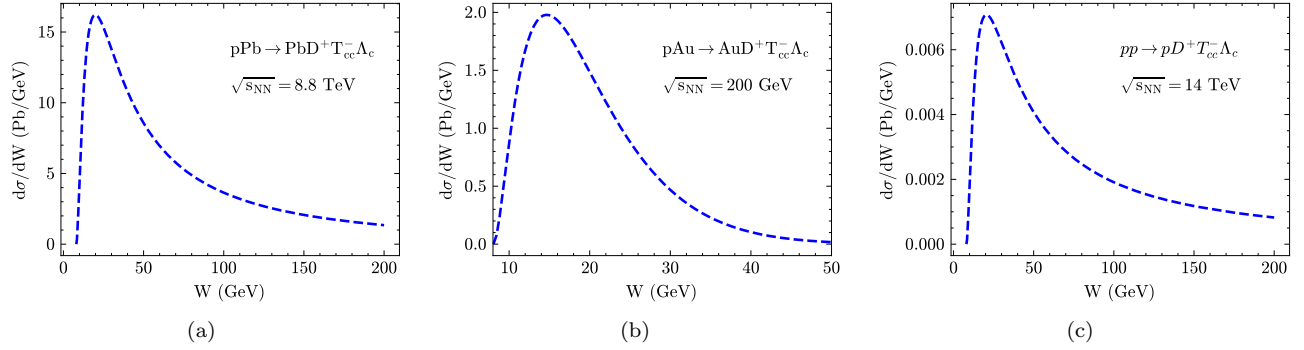


FIG. 4. Differential cross section as a function of W of one-photon T_{cc}^- production while subprocess is $\gamma p \rightarrow D^+T_{cc}^- \Lambda_c$ in p-Pb, p-Au, p-p UPCs respectively (from left to right).

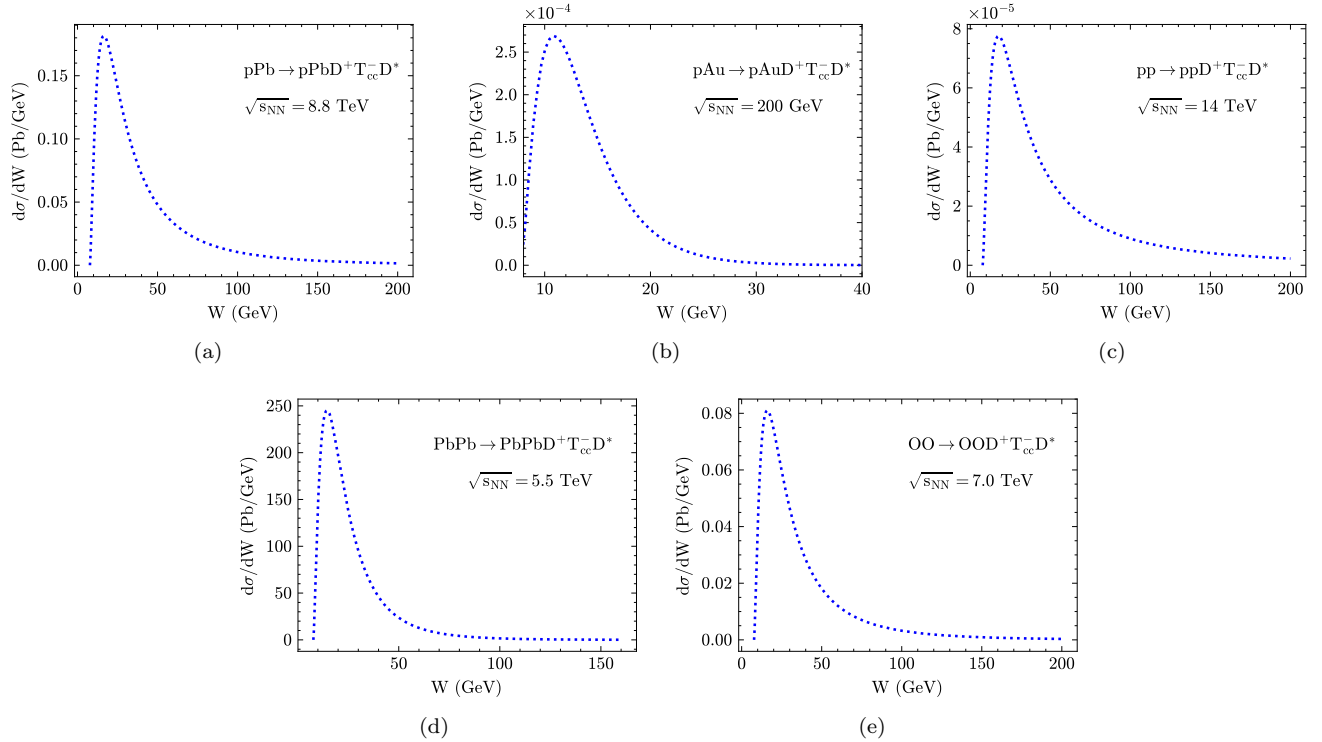


FIG. 5. The differential cross section $d\sigma/dW$ of two-photon T_{cc}^- production while subprocess is $\gamma\gamma \rightarrow D^+T_{cc}^-D^*$ in p-Pb, p-Au, p-p, Pb-Pb and O-O UPCs respectively.

TABLE I. 1. Integrated luminosity per typical run \mathcal{L}_{int} and c.m. energy $\sqrt{s_{NN}}$ of nucleus (proton) -nucleus (proton) UPCs from HL-LHC and RHIC [44, 50–52]. 2. The total cross sections and the events numbers of one-photon and two-photon T_{cc}^- production in different kinds of UPCs.

system	$\sqrt{s_{NN}}$	\mathcal{L}_{int} (pb^{-1})	σ_{tot} (pb)		events	
			one-photon	two-photon	one-photon	two-photon
Pb-Pb	5.5 TeV	5×10^{-3}	-	5191	-	25.9
O-O	7.0 TeV	12	-	2.5	-	30
Pb-p	8.8 TeV	1	1000	6.0	1000	6.0
Au-p	200 GeV	4.5	30.1	0.002	135.5	< 1
p-p	14 TeV	1.5×10^5	0.48	0.0035	7.2×10^4	525

the higher integrated luminosity per typical run \mathcal{L}_{int} in the p-p system, the event number is larger than that of the other processes. Conversely, it is noticeable that in the case of the two-photon process, the total cross-sections are smaller compared to those of the one-photon process in the Pb-p, Au-p, and p-p systems. Despite the total cross section σ_{tot} reaching approximately 5 nb for the two-photon T_{cc}^- process in the Pb-Pb system, owing to the very high two-photon number densities, the restricted luminosity results in a relatively small number of events. As a result, identifying T_{cc}^- through the one-photon process is more feasible.

IV. CONCLUSION

In this work, theoretical frameworks of one-photon and two-photon T_{cc}^- production are introduced. Then the differential distribution and the total cross section of one-photon and two-photon T_{cc}^- production in UPCs are calculated. At last, the events of T_{cc}^- production are estimated in different collision systems.

Based on the work of [19] for $\gamma p \rightarrow D^+ T_{cc}^- \Lambda_c$, the differential cross sections as a function of the center-of-mass energy of photon and proton (W) in Pb-p, Au-

p and p-p collisions are calculated. And Referring to $\gamma p \rightarrow D^+ T_{cc}^- \Lambda_c$ process, the t-channel amplitude of $\gamma\gamma \rightarrow D^+ T_{cc}^- D^*$ is presented. Then the differential cross sections for two-photon T_{cc}^- UPCs in different collision systems are shown. At last, the events of one-photon and two-photon T_{cc}^- production are estimated respectively. Due to high-luminosity photon flux in Pb-p and Pb-Pb systems, the total cross section of one-photon UPC process for T_{cc}^- production is approximately 1 nb and the total cross section of two-photon UPC process for T_{cc}^- production is approximately 5 nb respectively. But because of the limited integrated luminosity in Pb-p and Pb-Pb systems, the number of events is lower. In p-p system, despite the lower production cross-section of T_{cc}^- , the higher number of events is generated due to that the integrated luminosity is about $1.5 \times 10^5 \text{ Pb}^{-1}$. In conclusion, It is more possible to identify T_{cc}^- in p-p UPCs in the future HL-LHC.

ACKNOWLEDGMENTS

This work is supported by the Strategic Priority Research Program of Chinese Academy of Sciences under the Grant NO. XDB34030301.

-
- [1] F.-K. Guo, C. Hanhart, U.-G. Meißner, Q. Wang, Q. Zhao, and B.-S. Zou, *Rev. Mod. Phys.* **90**, 015004 (2018), [Erratum: *Rev.Mod.Phys.* 94, 029901 (2022)], arXiv:1705.00141 [hep-ph].
 - [2] H.-X. Chen, W. Chen, X. Liu, Y.-R. Liu, and S.-L. Zhu, *Rept. Prog. Phys.* **86**, 026201 (2023), arXiv:2204.02649 [hep-ph].
 - [3] S. K. Choi *et al.* (Belle), *Phys. Rev. Lett.* **91**, 262001 (2003), arXiv:hep-ex/0309032.
 - [4] M. Ablikim *et al.* (BESIII), *Phys. Rev. Lett.* **110**, 252001 (2013), arXiv:1303.5949 [hep-ex].
 - [5] Z. Q. Liu *et al.* (Belle), *Phys. Rev. Lett.* **110**, 252002 (2013), [Erratum: *Phys.Rev.Lett.* 111, 019901 (2013)], arXiv:1304.0121 [hep-ex].
 - [6] R. Aaij *et al.* (LHCb), *Phys. Rev. Lett.* **115**, 072001 (2015), arXiv:1507.03414 [hep-ex].
 - [7] R. Aaij *et al.* (LHCb), *Sci. Bull.* **66**, 1278 (2021), arXiv:2012.10380 [hep-ex].
 - [8] R. Aaij *et al.* (LHCb), *Nature Commun.* **13**, 3351 (2022), arXiv:2109.01056 [hep-ex].
 - [9] M. Albaladejo, *Phys. Lett. B* **829**, 137052 (2022), arXiv:2110.02944 [hep-ph].
 - [10] V. Montesinos, M. Albaladejo, J. Nieves, and L. Tolos, *Phys. Rev. C* **108**, 035205 (2023), arXiv:2306.17673 [hep-ph].
 - [11] M.-L. Du, V. Baru, X.-K. Dong, A. Filin, F.-K. Guo, C. Hanhart, A. Nefediev, J. Nieves, and Q. Wang, *Phys. Rev. D* **105**, 014024 (2022), arXiv:2110.13765 [hep-ph].
 - [12] S. S. Agaev, K. Azizi, and H. Sundu, *Nucl. Phys. B* **975**, 115650 (2022), arXiv:2108.00188 [hep-ph].
 - [13] L. Meng, G.-J. Wang, B. Wang, and S.-L. Zhu, *Phys. Rev. D* **104**, L051502 (2021).
 - [14] M.-J. Yan and M. P. Valderrama, *Phys. Rev. D* **105**, 014007 (2022), arXiv:2108.04785 [hep-ph].
 - [15] X.-Z. Ling, M.-Z. Liu, L.-S. Geng, E. Wang, and J.-J. Xie, *Phys. Lett. B* **826**, 136897 (2022), arXiv:2108.00947 [hep-ph].
 - [16] G.-J. Wang, Z. Yang, J.-J. Wu, M. Oka, and S.-L. Zhu, (2023), arXiv:2306.12406 [hep-ph].
 - [17] Y. Kim, M. Oka, and K. Suzuki, *Phys. Rev. D* **105**, 074021 (2022), arXiv:2202.06520 [hep-ph].
 - [18] E. J. Eichten and C. Quigg, *Phys. Rev. Lett.* **119**, 202002 (2017), arXiv:1707.09575 [hep-ph].
 - [19] Y. Huang, H. Q. Zhu, L.-S. Geng, and R. Wang, *Phys. Rev. D* **104**, 116008 (2021).
 - [20] A. Esposito, C. A. Manzari, A. Pilloni, and A. D. Polosa, *Phys. Rev. D* **104**, 114029 (2021), arXiv:2109.10359 [hep-ph].
 - [21] C. A. Bertulani, S. R. Klein, and J. Nystrand, *Ann. Rev. Nucl. Part. Sci.* **55**, 271 (2005), arXiv:nucl-ex/0502005.
 - [22] G. Baur, K. Hencken, D. Trautmann, S. Sadovsky, and Y. Kharlov, *Phys. Rept.* **364**, 359 (2002), arXiv:hep-ph/0112211.
 - [23] F. Krauss, M. Greiner, and G. Soff, *Prog. Part. Nucl. Phys.* **39**, 503 (1997).
 - [24] A. J. Baltz, *Phys. Rept.* **458**, 1 (2008), arXiv:0706.3356 [nucl-ex].
 - [25] E. J. Williams, *Phys. Rev.* **45**, 729 (1934).
 - [26] S. Uehara *et al.* (Belle), *Phys. Rev. Lett.* **96**, 082003 (2006), arXiv:hep-ex/0512035.
 - [27] S. Uehara *et al.* (Belle), *Phys. Rev. Lett.* **104**, 092001 (2010), arXiv:0912.4451 [hep-ex].
 - [28] C. P. Shen *et al.* (Belle), *Phys. Rev. Lett.* **104**, 112004 (2010), arXiv:0912.2383 [hep-ex].

- [29] S. R. Klein and Y.-P. Xie, *Phys. Rev. C* **100**, 024620 (2019), arXiv:1903.02680 [nucl-th].
- [30] Y.-P. Xie, X.-Y. Wang, and X. Chen, *Eur. Phys. J. C* **81**, 710 (2021), arXiv:2108.03767 [hep-ph].
- [31] S. R. Klein, J. Nystrand, J. Seger, Y. Gorbunov, and J. Butterworth, *Computer Physics Communications* **212**, 258 (2017).
- [32] Y.-P. Xie, X.-Y. Wang, and X. Chen, *Chin. Phys. C* **45**, 014107 (2021), arXiv:2007.11414 [hep-ph].
- [33] S. R. Klein and J. Nystrand, *Phys. Rev. C* **60**, 014903 (1999).
- [34] T. Lappi and H. Mantysaari, *Phys. Rev. C* **83**, 065202 (2011), arXiv:1011.1988 [hep-ph].
- [35] M. Drees and D. Zeppenfeld, *Phys. Rev. D* **39**, 2536 (1989).
- [36] Y. Dong, A. Faessler, T. Gutsche, S. Kumano, and V. E. Lyubovitskij, *Phys. Rev. D* **82**, 034035 (2010), arXiv:1006.4018 [hep-ph].
- [37] Y. Huang, J. He, J.-J. Xie, and L.-S. Geng, *Phys. Rev. D* **99**, 014045 (2019), arXiv:1610.06994 [hep-ph].
- [38] S. Okubo, *Phys. Rev. D* **11**, 3261 (1975).
- [39] P. D. G. Zyla, P A et al, *Progress of Theoretical and Experimental Physics* **2020**, 083C01 (2020).
- [40] A. Feijoo, W. H. Liang, and E. Oset, *Phys. Rev. D* **104**, 114015 (2021), arXiv:2108.02730 [hep-ph].
- [41] X.-D. Guo, D.-Y. Chen, H.-W. Ke, X. Liu, and X.-Q. Li, *Phys. Rev. D* **93**, 054009 (2016), arXiv:1602.02222 [hep-ph].
- [42] B. Aubert *et al.* (BaBar), *Phys. Rev. D* **76**, 111105 (2007), arXiv:hep-ex/0607083.
- [43] G. Pakhlova *et al.* (Belle), *Phys. Rev. D* **77**, 011103 (2008), arXiv:0708.0082 [hep-ex].
- [44] H.-S. Shao and D. d’Enterria, *JHEP* **09**, 248 (2022), arXiv:2207.03012 [hep-ph].
- [45] F.-K. Guo, C. Hanhart, Y. Kalashnikova, U.-G. Meißner, and A. Nefediev, *Physics Letters B* **742**, 394 (2015).
- [46] F.-K. Guo, C. Hanhart, U.-G. Meißner, Q. Wang, Q. Zhao, and B.-S. Zou, *Rev. Mod. Phys.* **90**, 015004 (2018).
- [47] M.-L. Du, V. Baru, F.-K. Guo, C. Hanhart, U.-G. Meißner, A. Nefediev, and I. Strakovsky, *Eur. Phys. J. C* **80**, 1053 (2020), arXiv:2009.08345 [hep-ph].
- [48] Y. Huang, C.-j. Xiao, Q. F. Lü, R. Wang, J. He, and L. Geng, *Phys. Rev. D* **97**, 094013 (2018).
- [49] J. C. Romao, “Computational techniques in quantum field theory,” <http://porthos.ist.utl.pt/CTQFT/>.
- [50] R. Bruce, D. d’Enterria, A. de Roeck, M. Drewes, G. R. Farrar, A. Giammanco, O. Gould, J. Hajer, L. Harland-Lang, J. Heisig, J. M. Jowett, S. Kabana, G. K. Krintiras, M. Korsmeier, M. Lucente, G. Milhano, S. Mukherjee, J. Niedziela, V. A. Okorokov, A. Rajantie, and M. Schaubmann, *Journal of Physics G: Nuclear and Particle Physics* **47**, 060501 (2020).
- [51] D. d’Enterria *et al.*, *J. Phys. G* **50**, 050501 (2023), arXiv:2203.05939 [hep-ph].
- [52] M. Tanabashi *et al.* (Particle Data Group), *Phys. Rev. D* **98**, 030001 (2018).